

Simulation of stress waves in attenuating drill strings, including piezoelectric sources and sensors

José M. Carcione^{a)} and Flavio Poletto

Istituto Nazionale di Oceanografia e di Geofisica Sperimentale (OGS), Borgo Grotta Gigante 42c, 34010 Sgonico, Trieste, Italy

(Received 10 February 1999; accepted for publication 4 April 2000)

A key element in drill steering and prediction of lithology ahead-of-the-bit is the transmission of while-drilling information from the bottom of the well to the rig operator and the geophysicists. Mud-pulse telemetry, based on pressure pulses along the drilling mud and extensional waves through the drill string, is the most used technique. The last method, properly designed, could transmit data rates up to 100 bits per second, against the 1 or 2 bits per second achieved with pressure pulses. In this work, a time-domain algorithm is developed for the propagation of one-dimensional axial, torsional, and flexural stress waves, including transducer sources and sensors. In addition, the equations include relaxation mechanisms simulating the viscoelastic behavior of the steel, dielectric losses, and any other losses, such as those produced by the presence of the drilling mud, the casing, and the formation. Moreover, the algorithm simulates the passbands and stopbands due to the presence of the coupling joints and pulse distortion and delay due to nonuniform cross-section areas. Acoustic and electric pulses, generated at one location in the string, can be propagated and detected at any other location by piezoelectric and acoustic sensors, such as PCB accelerometers, clamp-on ammeters, force, and strain transducers. © 2000 Acoustical Society of America. [S0001-4966(00)02907-6]

PACS numbers: 43.20.Mv, 43.40.Cw, 43.38.Fx, 43.20.Hq [DEC]

INTRODUCTION

Systems for transmitting information in a borehole involve electromagnetic radiation through the drill string and formations, the use of an insulated conducting cable, pressure pulses through the mud column, and acoustic wave propagation along the drill string. The most obvious technique, i.e., electrical transmission, would require stopping the drilling process every 10 m (a drill pipe segment) to add new electrical junctions. The only successful method is the transmission of pressure pulses, but this technique has a low transmission rate of about 2 bits per second. On the other hand, acoustic telemetry based on extensional waves along the drill string is a promising technique that, at present, is able to transmit 10 codified bits per second over a range of 1 km.^{1,2} Several patents have been presented on devices based on this telemetry technique, for instance, those issued by Hixon,³ Cox and Chaney,⁴ and Sharp and Smither.⁵

An important application of the acoustic telemetry method is the Seisbit[®] technology, which uses the extensional wave generated at the drill bit (the pilot signal detected at the rig) to obtain RVSP seismograms.^{6,7} Improvement of the method requires the understanding of signal transmission and attenuation of the main types of waves (extensional, torsional, and flexural) through the drill-string waveguide. At the frequencies used in hydrocarbon drilling, i.e., from 1 Hz to 2 kHz, longitudinal and torsional waves are nondispersive in a uniform pipe. However, in real drill strings, the propagation is affected by the presence of coupling joints, a nonuniform cross-sectional area, attenuation,

and drilling noise. The quasiperiodic structure of this waveguide generates a classical pattern of passbands and stop bands.³ For instance, extensional waves in a typical drill string have the first passband from 0 to 226 Hz and the first stop band from 226 to 280 Hz.¹ The ranges for torsional waves are 0 to 130 Hz and 130 to 176 Hz, respectively. Deviations from a perfect periodic structure and a variable cross section modify the location of these bands. In addition, other attenuation mechanisms act on the extensional waves. These include viscous dissipation into the drilling mud, conversion from extensional to torsional and flexural waves, and contact with the formation and well casing.

Besides waves from an acoustic source, such as the drill bit, it is important to transmit while-drilling information from piezoelectric transducer sources, located, for instance, in the bottom-hole assembly, to the drill rig on the surface. Both acoustic and electromagnetic energy can be transmitted through the waveguide if a constitutive equation based on piezoelectric coupling is assumed. In general, the signal wavelength is far greater than the 4.5-in diameter of the drill string, and the phenomenon can be accurately described by the one-dimensional wave equation.

In the present work, we develop a time-domain algorithm for the propagation of extensional, torsional, and flexural stress waves coupled with the electrostatic field equations, in order to include transducer sources and sensors. In addition, the equations include relaxation mechanisms simulating the viscoelastic behavior of the steel, dielectric losses, and any other losses, such as those produced by the presence of the drilling mud, the casing, and the formation. Moreover, the method, based on the one-dimensional (1D) wave equation, considers the presence of the coupling joints and nonuniform cross-section areas.

^{a)}Electronic mail: jcarcione@ogs.trieste.it

I. EXTENSIONAL WAVES

The analysis of wave propagation for a ferroelectric ceramic, classified as hexagonal crystal $6mm$, is performed in the Appendix. Propagation along the symmetry axis (direction of poling) implies the existence of coupled acoustic and electromagnetic waves and one stiffened acoustic wave, with elastic and electromagnetic polarizations directed along the symmetry axis. If we assume that the wavelength of the pulse propagating through the drill string is at least five times larger than the diameter of the string, the problem is one dimensional. In this case, the stiffened acoustic wave is the extensional wave propagating along the drill string.

Moreover, following Drumheller,⁹ we consider the presence of piezoelectric sources and sensors, and attenuation due to the viscoelastic properties of the steel, the presence of drilling mud, and other factors, like leaky modes.

A. The constitutive equations

Using the results obtained in the Appendix for a ferroelectric medium, the electric field E (E_3) denotes the axial component. The acoustic constitutive equation relates the axial (z)-component of the stress tensor, denoted by T_P (T_3), with the axial component of the strain tensor, denoted by S (S_3). The constitutive equations of the transducers, including electromagnetic losses, are

$$T_P = cS - eE, \quad D = eS + \epsilon * \partial_t E, \quad (1)$$

where D (D_3) is the electric displacement (nonzero in this case, since there are conduction currents), c (c_{33}) is the plane wave modulus, e (e_{z3}) is the piezoelectric coupling, and $\epsilon(t)$ (ϵ_{zz}) is the dielectric relaxation function (the symbol $*$ denotes time convolution).

The dielectric relaxation function includes one Debye mechanism, which is mathematically equivalent to a Zener model. Then

$$\epsilon = \epsilon^0 [1 - (1 - \alpha^2) \exp(-t\omega_1\alpha)] h(t), \quad \alpha = \sqrt{\epsilon^\infty / \epsilon^0}, \quad (2)$$

where ϵ^0 is the static permittivity, ϵ_∞ is the optical permittivity, ω_1 is the center frequency of the Debye peak, and h is the Heaviside function. Moreover, we should consider Ohm's law, relating the conduction current J_c to the electric field E ,

$$J_c = \sigma E, \quad (3)$$

where σ is the conductivity. We have neglected ferromagnetic relaxation, damping due to the piezoelectric coupling, and out-of-phase conduction currents.

The constitutive equation of the drill string can be written as

$$T_A = Y * \partial_t S, \quad Y = Y_1 + Y_2, \quad (4)$$

where the acoustic relaxation function Y_1 can be described by a Zener model, representing the string material, and a Maxwell model, representing additional dissipation factors, such as energy loss by radiation into the fluids which surround the drill string. The Zener relaxation function is

$$Y_1 = Y_0 [1 - (1 - \nu^2) \exp(-t\omega_0\nu)] h(t), \quad \nu = \sqrt{\frac{Y_U}{Y_0}}, \quad (5)$$

where Y_0 is the relaxed Young's modulus, Y_U is the unrelaxed Zener modulus, and ω_0 is the center frequency of the relaxation peak. The Maxwell relaxation function is simply

$$Y_2 = \eta Y_0 [\exp(-t/\tau) - 1] h(t), \quad (6)$$

where τ is the relaxation time and η is a dimensionless parameter. The unrelaxed or instantaneous contribution (i.e., when $t \rightarrow 0$ or $\omega \rightarrow \infty$) of the Maxwell relaxation function is zero, while the relaxed contribution (when $t \rightarrow \infty$ or $\omega \rightarrow 0$) is $-\eta Y_0$, so the relaxed modulus is $(1 - \eta) Y_0$.⁹

The transducer, described by the constitutive equations (1), is assembled in parallel to the metal part of the drill pipe, described by the constitutive equation (4). If the ratio of the transducer area to the total area is denoted by Θ , the total stress acting on this cross section is

$$T = (1 - \Theta) T_A + \Theta T_P = (1 - \Theta) Y * S + \Theta c S - \Theta e E, \quad (7)$$

since the parallel configuration implies that the strain is equal in both materials. Note that the system has an effective piezoelectric constant Θe .

B. The wave equation

The wave propagation problem is solved by introducing the balance of linear momentum and Maxwell's equations. Consider a small element PQ of length δz and let the cross-sectional area of the rod be $a(z)$. Continuity of particle velocity and force holds for a rod whose cross-sectional dimensions are small compared to the length of the rod (the stress can be double-valued or discontinuous). If the force on the face passing through P is F , the stress on the other face will be $F + (\partial_z F) \delta z$, and if v is the particle velocity of the element, Newton's second law implies

$$\rho a \delta z \partial_t v = \delta z \partial_z F. \quad (8)$$

On the other hand, the total force acting on the cross section of the drill string is

$$F = aT. \quad (9)$$

Introducing an acoustic source f , such as the drill bit, Eq. (8) can be rewritten as

$$\rho \partial_t v = a^{-1} \partial_z (aT) + f. \quad (10)$$

The material density $\rho(z)$ is given by

$$\rho = (1 - \Theta) \rho_1 + \Theta \rho_2, \quad (11)$$

where ρ_1 is the density of the drill string and ρ_2 is the density of the transducer.

Time convolutions in the constitutive equation (7) can be avoided by introducing memory variables.¹⁰ We obtain

$$T = [(1 - \Theta) Y_U + \Theta c] S + (1 - \Theta) Y_0 (\zeta_1 - \eta \zeta_2) - \Theta e E, \quad (12)$$

where the memory variables ζ_1 and ζ_2 satisfy

$$\partial_t \zeta_1 = -\omega_0 \nu [\zeta_1 - (1 - \nu^2) S] \quad (13)$$

and

$$\partial_t \zeta_2 = \frac{1}{\tau} (S - \zeta_2). \quad (14)$$

Since $\partial_t S = \partial_z v$, and redefining $\partial_t \zeta_l \rightarrow \zeta_l$, Eqs. (12)–(14) become

$$\begin{aligned} \partial_t T &= [(1 - \Theta)Y_U + \Theta c] \partial_z v \\ &\quad + (1 - \Theta)Y_0(\zeta_1 - \eta \zeta_2) - \Theta e \partial_t E, \\ \partial_t \zeta_1 &= -\omega_0 \nu [\zeta_1 - (1 - \nu^2) \partial_z v], \\ \partial_t \zeta_2 &= \frac{1}{\tau} (\partial_z v - \zeta_2), \end{aligned} \quad (15)$$

where we have used Eq. (9).

On the other hand, the radial-component of the electromagnetic equation in the transducer is,¹¹

$$0 = \sigma E + \partial_t D + J \quad (16)$$

[the generalized version of Eq. (A8i)], where J (J_r) is the electric current source.

Since part of the cross-sectional area consists of metal, we assume an effective piezoelectric coupling Θe . Taking this into account and introducing the hidden variable ξ ,¹² substitution of Eq. (1) into Eq. (16) yields

$$0 = \sigma_e E + \epsilon^\infty \partial_t E + \Theta e \partial_z v + \epsilon^0 \xi + J, \quad (17)$$

where

$$\sigma_e = \sigma + \omega_1 \alpha (1 - \alpha^2) \epsilon^0,$$

with ξ obeying the following first-order equation:

$$\partial_t \xi = -\omega_1 \alpha [\xi + \omega_1 \alpha (1 - \alpha^2) E]. \quad (18)$$

Time-differentiation of Eq. (17) gives

$$\sigma_e \mathcal{E} + \epsilon^\infty \partial_t \mathcal{E} + \Theta e \partial_z \partial_t v + \epsilon^0 \psi + \mathcal{J} = 0, \quad (19)$$

where $\mathcal{E} = \partial_t E$, $\psi = \partial_t \xi$, and $\mathcal{J} = \partial_t J$. Equation (10) implies $\partial_t v = [a^{-1} \partial_z a T + f] / \rho$. Substituting this expression into Eq. (19) we obtain

$$\sigma_e \mathcal{E} + \epsilon^\infty \partial_t \mathcal{E} + \Theta e \partial_z \left\{ \frac{1}{\rho} [a^{-1} \partial_z a T + f] \right\} + \epsilon^0 \psi + \mathcal{J} = 0, \quad (20)$$

which, together with the time derivative of (18),

$$\partial_t \psi = -\omega_1 \alpha [\psi + \omega_1 \alpha (1 - \alpha^2) \mathcal{E}], \quad (21)$$

forms the electromagnetic equations.

C. Plane wave solution

Let us assume a harmonic wave with a phase factor $\exp(i\omega t)$, where ω is the angular frequency. Then, the constitutive equations (1) and (4) can be written as

$$\begin{aligned} T_p &= cS - eE, \\ D &= eS + \tilde{\epsilon}E, \end{aligned} \quad (22)$$

$$T_A = \tilde{Y}S,$$

where

$$\tilde{Y} = \nu Y_0 \frac{\omega_0 + i\omega \nu}{\omega_0 \nu + i\omega} - \frac{\eta Y_0}{1 + i\omega \tau} \quad (23)$$

and

$$\tilde{\epsilon} = \alpha \epsilon_0 \frac{\omega_1 + i\omega \alpha}{\omega_1 \alpha + i\omega}. \quad (24)$$

Now, assume a plane wave with a particle velocity having an spatial phase factor $\exp(-i\omega s z)$, where s is the complex slowness (this quantity is complex in the lossy case; the real and imaginary parts are related to the wave number and the attenuation, respectively). For any field variable, we have $\partial_z \rightarrow -i\omega s$. It is easy to show that the dispersion equation is

$$s^2 \left[(1 - \Theta) \tilde{Y} + \Theta c + \frac{(\Theta e)^2}{\epsilon^*} \right] = \rho, \quad (25)$$

where

$$\epsilon^* = \tilde{\epsilon} - \frac{i}{\omega} \sigma. \quad (26)$$

The physical phase velocity and attenuation factor are given by

$$V_p = [\text{Re}(s)]^{-1} \quad (27)$$

and

$$\bar{\alpha} = -\omega \text{Im}(s), \quad (28)$$

respectively.

D. Wave equation in matrix form

Equations (20) and (21), together with Eqs. (10) and (15), form the wave equation in the quasistatic case. Note that $\partial_t E$ must be replaced by the variable \mathcal{E} in Eq. (15). These equations govern solutions that travel at velocities comparable to acoustic velocities.

The quasistatic differential equations can be written in matrix form as

$$\partial_t \mathbf{w} = \mathbf{M} \mathbf{w} + \mathbf{s}, \quad (29)$$

where

$$\mathbf{w} = [v, T, \zeta_1, \zeta_2, \mathcal{E}, \psi]^\top \quad (30)$$

is the unknown vector,

$$\mathbf{s} = [f/\rho, 0, 0, 0, -[\mathcal{J} + \Theta e \partial_z (\rho^{-1} f)]/\epsilon^\infty, 0]^\top \quad (31)$$

is the source vector, and \mathbf{M} is the propagation matrix, given by

$$\mathbf{M} = \begin{pmatrix} 0 & M_{12} & 0 & 0 & 0 & 0 \\ M_{21} & 0 & M_{23} & M_{24} & M_{25} & 0 \\ M_{31} & 0 & M_{33} & 0 & 0 & 0 \\ M_{41} & 0 & 0 & M_{44} & 0 & 0 \\ 0 & M_{52} & 0 & 0 & M_{55} & M_{56} \\ 0 & 0 & 0 & 0 & M_{65} & M_{66} \end{pmatrix}, \quad (32)$$

where

$$\begin{aligned} M_{12} &= (\rho a)^{-1} \partial_z a, \\ M_{21} &= [(1 - \Theta)Y_U + \Theta c] \partial_z, \quad M_{23} = (1 - \Theta)Y_0, \\ M_{24} &= -(1 - \Theta)\eta Y_0, \quad M_{25} = -e\Theta, \\ M_{31} &= \omega_0 \nu (1 - \nu^2) \partial_z, \quad M_{33} = -\omega_0 \nu, \end{aligned} \quad (33)$$

$$M_{41} = \tau^{-1} \partial_z, \quad M_{44} = -\tau^{-1},$$

$$M_{52} = -\frac{\Theta e}{\epsilon^\infty} \partial_z (\rho a)^{-1} \partial_z a, \quad M_{55} = -\sigma_e / \epsilon^\infty,$$

$$M_{56} = -\epsilon^0 / \epsilon^\infty, \quad M_{65} = -\omega_1^2 \alpha^2 (1 - \alpha^2), \quad M_{66} = -\omega_1 \alpha.$$

II. TORSIONAL WAVES

The constitutive equation for torsional waves in a ferroelectric ceramic is similar to that of the extensional waves, given in Eq. (1). For torsional vibrations, E denotes the azimuthal component E_ϕ of the electric field, T_ρ is the ϕz -component of the piezoelectric stress tensor, S is the ϕz -component of the strain tensor, D is the azimuthal component (D_ϕ) of the electric displacement, c is the rigidity modulus c_{44} , e is the piezoelectric coupling (e_{x5}), and $\epsilon(t)$ is the dielectric relaxation function $\epsilon_{11}(t)$. As before, the acoustic relaxation function $c_{44}(t)$ of the drill string (Y for extensional waves) can be described by a parallel connection between a Zener model and a Maxwell model, representing additional dissipation factors. Similarly, a Debye mechanism represents the dielectric relaxation function.

The wave propagation problem is solved by introducing the balance of angular momentum^{13,14} and Maxwell's equations. Let ϕ denote the relative angular displacement of two cross sections, so that $\partial_z \phi$ is the twist of the cylinder. The torsional couple is equal to the radius of gyration R_T multiplied by the force aT , i.e., $C = aR_T T$, where T is the ϕz -component of the total stress tensor. The moment of the kinetic reactions about the axial axis $\rho a R_T^2 \partial_{tt} \phi$ balances the angular moment $\partial_z C$. Then, the equation of motion is

$$\rho a R_T^2 \partial_{tt} \phi = \partial_z (a R_T T). \quad (34)$$

Note that the radius of gyration is defined by

$$R_T^2 = a^{-1} \int d^2 da \quad (35)$$

(Ref 15), where d is the distance to the axis of rotation. For a hollow cylinder, the radius of gyration, with respect to the axial axis z , is

$$R_T = \frac{1}{\sqrt{2}} (r_1^2 + r_2^2)^{1/2}, \quad (36)$$

where r_1 and r_2 are the inner and outer radii, respectively. Defining $\Omega = \partial_t \phi$ and the polar moment of inertia per unit mass,

$$I = a R_T^2 = \frac{\pi}{2} (r_2^4 - r_1^4), \quad (37)$$

Eq. (34) becomes

$$\rho \partial_t \Omega = I^{-1} \partial_z (I \hat{T}) + f_T, \quad (38)$$

where $\hat{T} = T/R_T$ (it is assumed that the ϕ -displacement is equal to $R_T \phi$), and we have introduced the external torque f_T . The time derivative of the constitutive equation is

$$R_T \partial_t \hat{T} = [(1 - \Theta) Y_U + \Theta c] \partial_z R_T \Omega + (1 - \Theta) Y_0 (\zeta_1 - \eta \zeta_2) - \Theta e \mathcal{E}, \quad (39)$$

where, for simplicity, we use the same notation as for the extensional waves. Here, Y_0 and Y_U denote the relaxed and unrelaxed limits of the drill-string relaxation function c_{44} , and ζ_1 is the corresponding hidden variable, with v replaced by $R_T \Omega$ in Eq. (15). The same argument holds for the parameters of the Maxwell model.

In matrix notation, the equation describing torsional oscillations, coupled with the quasistatic electromagnetic field, has the form (26), where

$$\mathbf{w} = [\Omega, \hat{T}, \zeta_1, \zeta_2, \mathcal{E}, \psi]^\top \quad (40)$$

is the unknown vector,

$$\mathbf{s} = [f_T / \rho, 0, 0, 0, -[\mathcal{J} + \Theta e \partial_z (R_T \rho^{-1} f_T)] / \epsilon^\infty, 0]^\top \quad (41)$$

is the source vector, and \mathbf{M} is the propagation matrix, whose components have the same expression (33), except for

$$\begin{aligned} M_{12} &= (I\rho)^{-1} \partial_z I, & M_{21} &= [(1 - \Theta) Y_U + \Theta c] R_T^{-1} \partial_z R_T, \\ M_{23} &= (1 - \Theta) R_T^{-1} Y_0, & M_{24} &= -(1 - \Theta) R_T^{-1} \eta Y_0, \\ M_{25} &= -\Theta R_T^{-1} e, \\ M_{31} &= \omega_0 v (1 - v^2) \partial_z R_T, \\ M_{41} &= \tau^{-1} \partial_z R_T, \\ M_{52} &= -\frac{\Theta e}{\epsilon^\infty} \partial_z R_T (\rho I)^{-1} \partial_z I. \end{aligned} \quad (42)$$

It can be shown that the dispersion relation has the form (25).

III. FLEXURAL WAVES

In the simplest theory of flexural vibrations it is assumed that the motion of each element of the pipe is purely one of translation in a direction perpendicular to the axis of the pipe. We assume that the wavelength is much larger than the diameter of the drill string. Therefore, effects such as rotary inertia are neglected.^{13,14} Following Kolsky,¹⁴ the equation of motion for flexural vibrations of bars is

$$\rho a \partial_{tt} w = -\partial_z \mathcal{F} + f_F, \quad (43)$$

where w is the displacement in the plane of bending [e.g., if (x, z) is the bending plane, w points in the x -direction], f_F is the external force, and \mathcal{F} is the shearing force. This is given by

$$\mathcal{F} = -\partial_z M = \partial_z (a R_F^2 Y_U \partial_{zz} w), \quad (44)$$

where M is the bending moment, Y_U is the unrelaxed Young modulus, and R_F is the radius of gyration of the cross section about an axis through its centroid at right angles to the plane of bending. For the (x, z) -plane $R_F^2 = a^{-1} \int x^2 da$, which for a hollow cylinder is

$$R_F = \frac{1}{2} (r_1^2 + r_2^2)^{1/2}. \quad (45)$$

Coupling with the axial force F implies additional terms in Eqs. (43) and (10). Chin¹⁶ (pp. 225, 257, and 271). Including these interactions and since $F = aT$, Eqs. (10) and (43) become

$$a \rho \partial_t v = \partial_z F + a Y_U R_F^2 \partial_z [(\partial_{zzz} w)(\partial_z w)] + a f \quad (46)$$

and

$$\rho a \partial_{tt} w = -\partial_z(\mathcal{F} + F \partial_z w) + f_F, \quad (47)$$

with F given by Eq. (9). Coupling with the axial motion allows the inclusion of losses and piezoelectric effects.

On the other hand, assuming a large bending radius, Drummheller¹⁷ obtains the following coupled differential equations:

$$\rho a \partial_t v = \partial_z F - \frac{\mathcal{F}}{r_b} + af \quad (48)$$

and

$$\rho a \partial_{tt} w = -\partial_z \mathcal{F} - \frac{F}{r_b} + f_F, \quad (49)$$

where r_b is the radius of curvature of the string (bending radius). Assuming no loss for simplicity, the stress is¹⁷

$$T = [(1 - \Theta) Y_U + \Theta c] \left(S + \frac{w}{r_b} \right) + \Theta e E, \quad (50)$$

where $Y_U = Y_0$.

Let $\hat{x}(z)$ denote the reference line of the string. The condition $\hat{x}(z) = 0$ defines a straight string. For large bending radius,

$$\partial_{zz} \hat{x} = \frac{1}{r_b(z)}. \quad (51)$$

Since $\partial_z(F \partial_z w)$ in Eq. (47) is equal to $\partial_z F \partial_z w + F \partial_{zz} w$, Eqs. (47) and (49) are equivalent if $\partial_z F \partial_z w$ can be neglected and $\partial_{zz} w \approx \partial_{zz} \hat{x} = 1/r_b$. Similarly, Eq. (46) is equivalent to Eq. (48) if $(\partial_{zzzz} w)(\partial_z w)$ can be neglected and $\partial_{zz} w \approx 1/r_b$. However, note that the presence of a radius of curvature implies the action of a lateral force f_F in Eq. (47), otherwise there is no coupling between the flexural and axial motions when solving the problem with Eqs. (46) and (47).

Moreover, the drill string is prestressed by its weight, but in order to avoid collapse, it is lifted at the surface, where it is in tension. Since it must contact the formation in order to drill, it is in compression at the bit. Hence, the static axial load changes from tension at the surface to compression at the bit, with the point of zero stress close to the drill collar. Assuming $z=0$ at the bit and that the distance to the neutral point is z_N , the force per unit area of drill string is

$$N = a \rho g (z - z_N), \quad (52)$$

where g is the acceleration of gravity. In terms of the *weight-on-bit* (WOB), the force is $N = a \rho g z - \text{WOB}$ ¹⁶ (p. 145). The axial force satisfies $N < 0$ for the segments in tension, and $N > 0$ for the segments in compression. The transition $N = 0$ defines the neutral point of the drill string. When modeling gravity effects, the force N should be added to the axial force F in Eqs. (47)–(49).

Plane wave analysis

Let us consider a uniform drill string subject to the variable axial force N and assume that there is no coupling with the extensional wave. Substitution of Eq. (44) into (47) with $F=0$ yields

$$\rho a \partial_{tt} w + a R_F^2 Y \partial_{zzzz} w + \partial_z(N \partial_z w) = 0, \quad (53)$$

where we assume that there are no external forces. A plane wave ansatz $\exp i(kx - \omega t)$, where k is the complex wave number, gives the following dispersion equation:¹⁶

$$\rho a \omega^2 = a R_F^2 Y k^4 - N k^2 + i k \partial_z N. \quad (54)$$

Using Eq. (52) and $\partial_z N = a \rho g$, we get

$$\rho \omega^2 = R_F^2 Y k^4 - \rho g (z - z_N) k^2 + i k \rho g. \quad (55)$$

Equation (55) has four solutions, with phase velocity and attenuation factor given by

$$V_p = \omega [\text{Re}(k)]^{-1}, \quad \bar{\alpha} = -\text{Im}(k), \quad (56)$$

respectively. The group velocity is equal to the derivative of the angular frequency with respect to the real part of k . It gives

$$V_g = \left[\text{Re} \left(\frac{\partial k}{\partial \omega} \right) \right]^{-1}. \quad (57)$$

From Eq. (55) we obtain

$$\frac{\partial k}{\partial \omega} = 2 \rho \omega [4 R_F^2 Y k^3 - 2 k \rho g (z - z_N) + i \rho g]^{-1}. \quad (58)$$

IV. THE ALGORITHMS

Previous algorithms for computing drill-string axial motion use the method of characteristics and low-order finite differencing,¹⁸ and frequency-domain techniques.¹⁹ Here, drill-string axial, torsional, and lateral vibrations are computed with a fourth-order Runge-Kutta technique. The method calculates the field at time $(n+1)dt$, where dt is the time step, as

$$\mathbf{w}^{n+1} = \mathbf{w}^n + \frac{dt}{6} (\Delta_1 + 2\Delta_2 + 2\Delta_3 + \Delta_4), \quad (59)$$

where

$$\Delta_1 = \mathbf{M} \mathbf{w}^n + \mathbf{s}^n,$$

$$\Delta_2 = \mathbf{M} \left(\mathbf{w}^n + \frac{dt}{2} \Delta_1 \right) + \mathbf{s}^{n+1/2},$$

$$\Delta_3 = \mathbf{M} \left(\mathbf{w}^n + \frac{dt}{2} \Delta_2 \right) + \mathbf{s}^{n+1/2},$$

$$\Delta_4 = \mathbf{M} (\mathbf{w}^n + dt \Delta_3) + \mathbf{s}^{n+1}.$$

The spatial derivatives are calculated with the Fourier and Chebyshev methods by using the fast Fourier transform (FFT).^{20,21} These approximations are infinitely accurate for band-limited periodic functions with cutoff spatial wave numbers which are smaller than the cutoff wave numbers of the mesh. When using the Chebyshev method, nonperiodic boundary conditions can be implemented at the end of the pipes, and the grid points can be distributed in accordance with the structure and geometry of the drill string. We consider the following coordinate transformation from the computational to the physical domain:

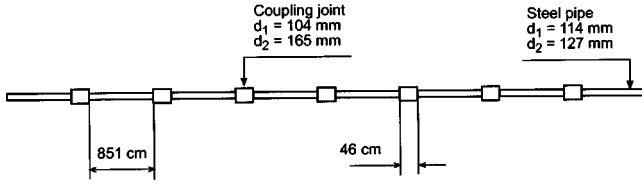


FIG. 1. Regular drill string consisting of pipes and tool joints.

$$z_j = z_{\max} \frac{q(\xi_j) - q(-1)}{q(1) - q(-1)}, \quad j=0, \dots, n_z - 1, \quad (60)$$

mapping the interval $[-1, 1]$ onto the interval $[0, z_{\max}]$, where $\xi_j = \cos[\pi j / (n_z - 1)]$ are the Gauss-Lobatto collocation points. The function

$$q = q(\xi, \alpha) \quad (61)$$

is a family of transformations, where α is a vector of parameters defining the mapping. The spatial derivative of a field variable in the physical domain is then given by

$$\frac{\partial u}{\partial z} = \frac{\partial u}{\partial \xi} \frac{\partial \xi}{\partial z} = \left[\frac{q(1) - q(-1)}{z_{\max}} \right] \frac{\partial \xi}{\partial q} \frac{\partial u}{\partial \xi}. \quad (62)$$

For instance, in the second example we use the following symmetric mapping function:

$$q(\xi) = \frac{\arcsin(\gamma \xi)}{\arcsin(\gamma)}, \quad (63)$$

satisfying $q(1) = 1$ and $q(-1) = -1$. Here $\alpha = \gamma$, and

$$\frac{\partial \xi}{\partial q} = \frac{\arcsin(\gamma)}{\gamma} \sqrt{1 - \gamma^2 \xi^2}. \quad (64)$$

This mapping stretches the mesh at the boundaries. When $\gamma \rightarrow 0$, we obtain the Gauss-Lobatto collocation points, and $\gamma \rightarrow 1$ gives equally distributed points as in the Fourier differential operator. Using this mapping, the spatial derivative (62) can be rewritten as

$$\frac{\partial u}{\partial z} = \frac{1}{\gamma dz} \arcsin \left[\gamma \sin \left(\frac{\pi}{n} \right) \right] \sqrt{1 - \gamma^2 \xi^2} \frac{\partial u}{\partial \xi}, \quad (65)$$

where n_z is the number of grid points, and dz is the maximum grid spacing.

Free surface boundary conditions at the end of the pipes are implemented by the technique described in Ref. 21.

V. EXAMPLES

A. Propagation of extensional stress waves along an attenuating drill string with periodic coupling joints

A drill string with the characteristics shown in Fig. 1 is used to simulate acoustic transmission through nine pipe elements separated by ten tool joints. In particular, this problem has been solved by Drumheller¹⁸ with a different numerical algorithm, based on the method of finite differences. The Young modulus of the pipe and coupling joints is $Y_U = Y_0 = 206$ GPa, and the material density is $\rho = 7850$ kg/m³. We consider $n_z = 3465$ and a uniform grid spacing $dz = 23$ cm. The source time history is

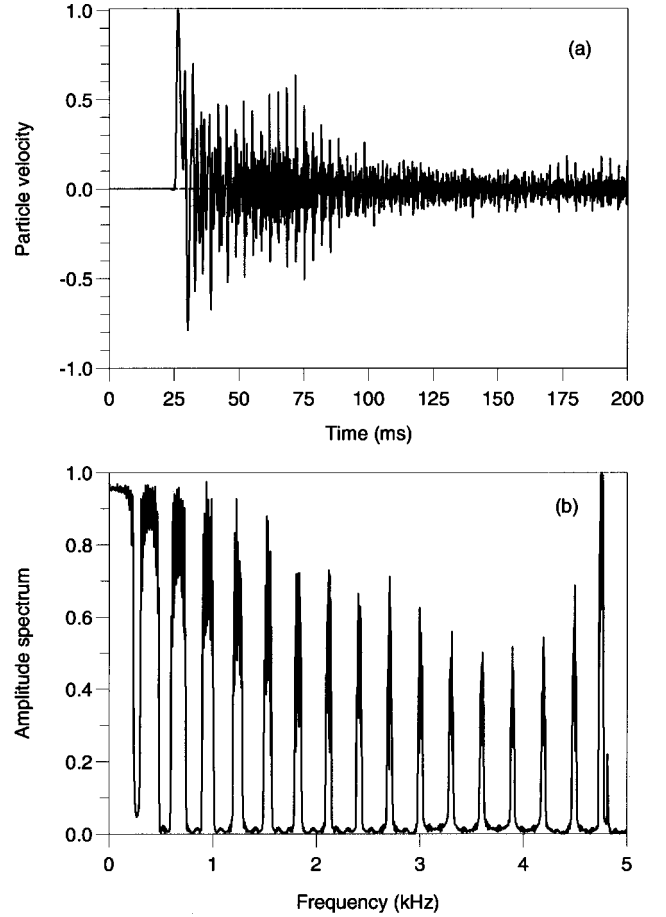


FIG. 2. Time history (a) and Fourier transform (b) of the sinc extensional pulse propagated along ten tool joints (see Fig. 1).

$$f(t) = \text{sinc}[2\pi f_c(t - t_0)],$$

which corresponds to a gate function in the frequency domain. The source frequency is 5.568 kHz, which is half the maximum frequency “supported” by the mesh, i.e., $f_{\max} = V_{p \min} / (2dz)$, where $V_{p \min}$ is the minimum phase velocity. Frequencies beyond this limit are aliased. The source is located at grid point 1499 and the receiver at grid point 2050. The first tool joint starts at grid point 1599, with each joint modeled by two grid points and each pipe element by 37 grid points. The spatial derivatives are computed with the Fourier method, and absorbing regions of length 18 grid points are implemented at the two ends of the drill string to avoid wrap-around effects. The wave field is computed by using a time step of $1 \mu\text{s}$, with the time history resampled every $40 \mu\text{s}$.

Figure 2 shows the time history (a) and its Fourier transform (b), where the characteristic passbands can be appreciated.^{1,8} The transform was made using a sampling interval of $40 \mu\text{s}$ and 5544 points.

The following numerical experiment considers the band-limited time function

$$f(t) = \exp \left[-\frac{1}{2} f_c^2 (t - t_0)^2 \right] \cos[\pi f_c (t - t_0)], \quad (66)$$

where f_c is the cutoff frequency and $t_0 = 3/f_c$.

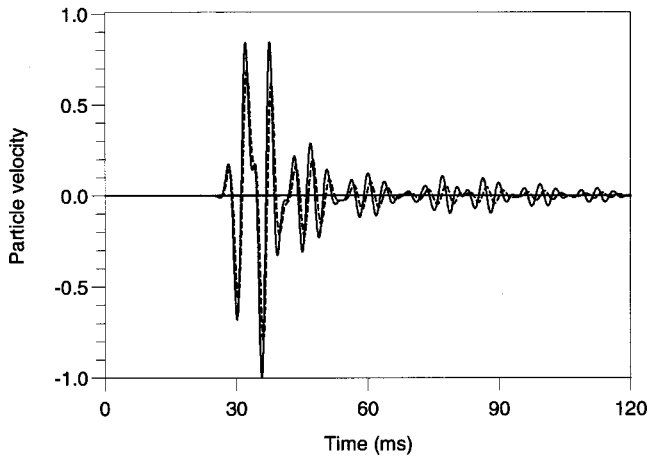


FIG. 3. Time history for extensional waves corresponding to the model illustrated in Fig. 1, showing the case without loss (continuous line) and with loss (broken line).

Attenuation can be easily parameterized as a function of the minimum quality factor Q of the relaxation peak and the central frequency f_0 of this peak. We have

$$Q = \frac{2\nu}{\nu^2 - 1} \quad \text{and} \quad f_0 = \frac{\omega_0}{2\pi}.$$

We assume $f_c = 500$ Hz, $Q = 200$, $f_0 = f_c/2$, and Maxwell's parameters $\eta = 0.02$ and $\tau = 200$ μ s, which are used to model the radiated energy into the fluids surrounding the drill string. Figure 3 compares the time histories corresponding to the lossless (continuous line) and lossy (broken line) cases. As expected, the attenuation is more pronounced for the coda waves.

B. Transmission of extensional pulses between ferroelectric ceramics

In this example we consider the propagation of stress waves between two piezoelectric transducers joined by a hollow cylinder made of brass. The model and configuration, shown in Fig. 4, correspond to a laboratory experiment conducted by Drumheller.⁹ The Young modulus of the cylinder is $Y_U = Y_0 = 108.13$ GPa, and its material density is $\rho = 8456$ Kg/m³. Intrinsic loss in the brass is described by the Zener model with $Q = 180$ and $f_0 = 20$ KHz.

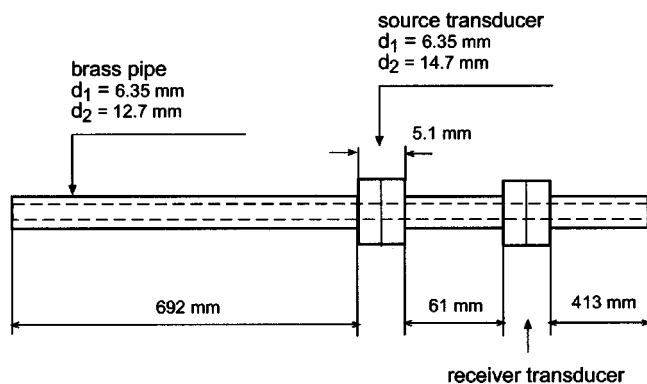


FIG. 4. Geometry of the experiment corresponding to the ferroelectric transducers (not in scale). Both ends of the brass pipe satisfy free surface boundary conditions.

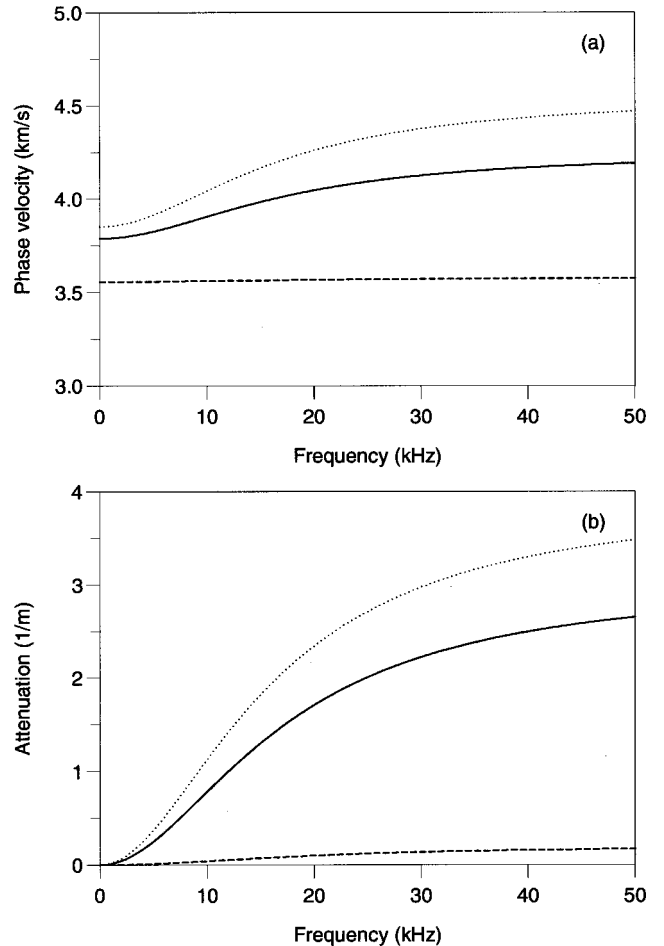


FIG. 5. Phase velocity (a) and attenuation factor (b) of a wave propagating in an assemble brass/ferroelectric ceramic (continuous line), where the proportion of ceramic is $\Theta = 0.8$. The broken line corresponds to the pure brass material (i.e., $\Theta = 0$) and the dashed line to the pure ceramic material (i.e., $\Theta = 1$).

As in the acoustic case, dielectric loss is parameterized by the minimum quality factor Q_e and the central frequency f_1 of the relaxation peak. We have

$$Q_e = \frac{2\alpha}{\alpha^2 - 1} \quad \text{and} \quad f_1 = \frac{\omega_1}{2\pi}.$$

The source transducer is made of lead titanate-zirconate (PZT-5H ceramic) whose properties^{9,11} are $c = 48.24$ GPa, $\rho = 7489$ kg/m³, $e = 23.3$ C/m², $\epsilon^0 = 1470 \epsilon_0$, $Q_e = 50$, $f_1 = 20$ kHz, and $\sigma = 1.5$ mS/m. On the other hand, the receiver transducer (also PZT-5H ceramic) has acoustic properties $c = 111$ GPa, $\rho = 7485.3$ kg/m³, and similar electric properties to the source transducer. These data are in agreement with Table IV of Ref. 9. Figure 5 shows the phase velocity (27) (a) and attenuation factor (28) (b) as a function of frequency for the receiver transducer. The continuous line corresponds to a wave propagating in an assemble of brass/ferroelectric ceramic, where the proportion of ceramic is $\Theta = 0.8$, while the broken line corresponds to the pure brass material (i.e., $\Theta = 0$) and the dashed line to the pure ceramic material (i.e., $\Theta = 1$).

We consider $n_z = 694$ and a uniform grid spacing $dz = 1.745$ mm. The source transducer is located between grid

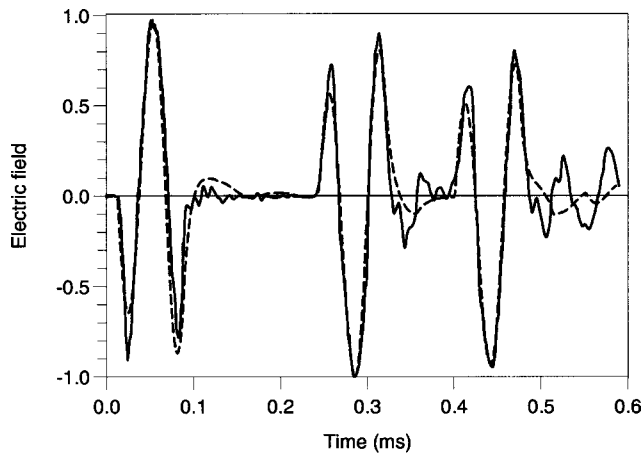


FIG. 6. Time history of an extensional pulse propagated between two piezoelectric transducers (see Fig. 4) (broken line) compared to the experimental results obtained by Drumheller (Ref. 9) (continuous line).

points 407 and 410, and the electric current is applied to grid point 408. The time history of the source, $\mathcal{J}(t)$, is given in Fig. 9 of Drumheller.⁹ The receiver transducer is located between grid points 446 and 449, and the signal is recorded at grid point 447. The spatial derivatives are computed with the Chebyshev method, using the mapping function (63) with $\gamma=0.999$. Free surface boundary conditions are satisfied by the two ends of the brass cylinder. The wave field is com-

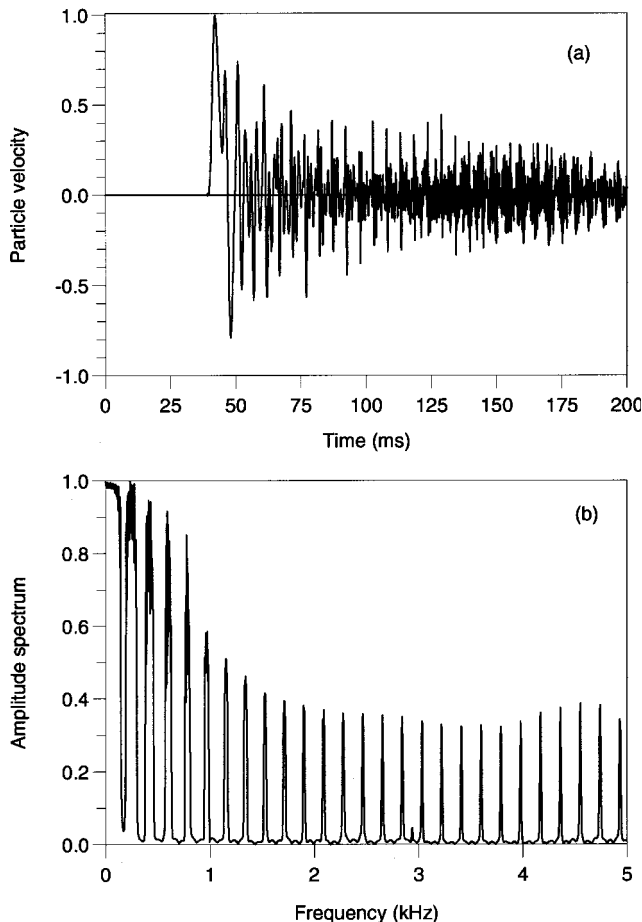


FIG. 7. Time history (a) and Fourier transform (b) of the sinc torsional pulse propagated along ten tool joints (see Fig. 1).

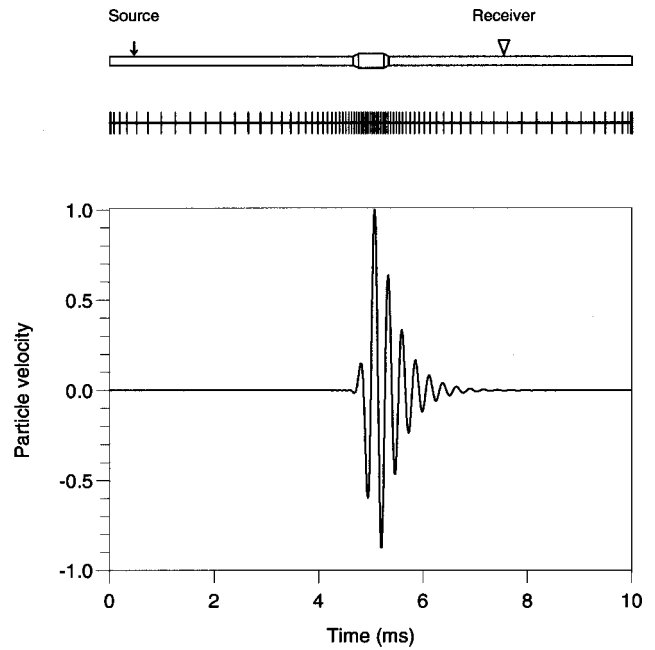


FIG. 8. Section of drill string, numerical mesh, and time history of the angular velocity Ω for torsional waves propagating from source to receiver.

puted by using a time step of $0.1 \mu\text{s}$, with the time history resampled every $1.6 \mu\text{s}$.

The time history of the electric field at the receiver transducer is illustrated in Fig. 6 (broken line) and compared to the experimental results (continuous line). The first pulse is the direct signal traveling from source to receiver. The second and third pulses are the reflections off the right and left boundaries, respectively.

C. Transmission of torsional stress waves

The drill string shown in Fig. 1 is used to simulate transmission of torsional waves. The rigidity modulus of the pipe and coupling joints is $Y_U=Y_0=82.4 \text{ GPa}$. The same mesh and modeling parameters of the previous example are used here. Figure 7 shows the time history (a) (Ω) and its Fourier transform (b). As before, the transform was made using a sampling interval of $40 \mu\text{s}$ and 5544 points.

The following simulation uses the Chebyshev differential operator and a mapping transformation to model in detail the geometrical features of the coupling joints, while using a coarse distribution of grid points for modeling the pipes (see Fig. 8). For simplicity, we consider propagation through one coupling joint. The Gauss-Lobatto collocation points are redistributed by using the following mapping function:

$$q(\zeta) = \frac{2}{\pi} \arctan[\varepsilon \tan(\varphi)], \quad \varphi = \frac{\pi\zeta}{2}, \quad (67)$$

with $\varepsilon=0.2$, satisfying $q(1)=1$ and $q(-1)=-1$, and

$$\frac{\partial\zeta}{\partial q} = \frac{1}{\varepsilon} [\cos^2(\varphi) + \varepsilon^2 \sin^2(\varphi)]. \quad (68)$$

Equation (67) is a particular case of the transformation used in Ref. 21. Using this mapping, the spatial derivative (62) can be rewritten as

$$\frac{\partial u}{\partial z} = \frac{2}{\varepsilon z_{\max}} [\cos^2(\varphi) + \varepsilon^2 \sin^2(\varphi)] \frac{\partial u}{\partial \zeta}, \quad (69)$$

where z_{\max} is the length of the string.

We consider $n_z = 309$, a string length $z_{\max} = 20.5$ m, and a source time-history with dominant frequency $f_d = 4$ kHz. The diameters of the pipes and joint are those illustrated in Fig. 1, but with a linear transition from grid point 144 (10.02 m) to 147 (10.08 m) (from pipe to joint) and from point 163 (10.42 m) to 166 (10.48 m) (from joint to pipe). Figure 8 shows the string and the numerical mesh, where one grid point every four is represented. The source is located at grid point 20 (0.95 m) and the receiver at grid point 260 (15.46 m). At the two ends of the string, nonreflecting boundary conditions based on the method of characteristics are imposed²¹ and, in addition, absorbing strips of length 18 are implemented to avoid any spurious reflection. The time-history, computed with a time step of $1 \mu\text{s}$ and resampled to $10 \mu\text{s}$, is shown in Fig. 8. A set of coupling joints can be modeled by a general transformation based on functions of the type given in Eq. (67).

D. Propagation of flexural waves

The simulation of flexural waves requires a careful analysis of the dispersion equation. In order to avoid aliasing, the source spectrum must be band-limited, with the minimum frequency strictly greater than zero. This will be illustrated in the following analysis. According to the sampling theorem the maximum frequency allowed by the mesh is

$$f_{\max} = \frac{V_{p \min}}{2dz},$$

where $V_{p \min}$ is the minimum phase velocity obtained from Eq. (56),

$$V_{p \min} = 2\pi f_{\min} [\text{Re}(k(f_{\min}))]^{-1},$$

with f_{\min} the minimum frequency of the spectrum. Then, the minimum allowable dz is

$$dz_{\min} = \frac{\pi f_{\min} [\text{Re}(k(f_{\min}))]^{-1}}{f_{\max}}.$$

Neglecting gravity forces ($N=0$) and coupling with the axial force ($F=0$) we obtain

$$dz_{\min} = \frac{\sqrt{\pi R_F c_0 f_{\min}}}{\sqrt{2} f_{\max}},$$

where $c_0 = \sqrt{Y/\rho}$.

Let us consider the example illustrated in Fig. 1 with $N=F=0$. The perturbation is initiated by the flexural force f_F , with a time history whose frequency spectrum is a Butterworth filter having a minimum frequency of 50 Hz and a maximum frequency of 570 Hz (computed for the pipe section), corresponding to a grid spacing $dz = 23$ cm. The wavelet and its Fourier transform are illustrated in Figs. 9(a) and 9(b), respectively.

The dispersion equation (55),

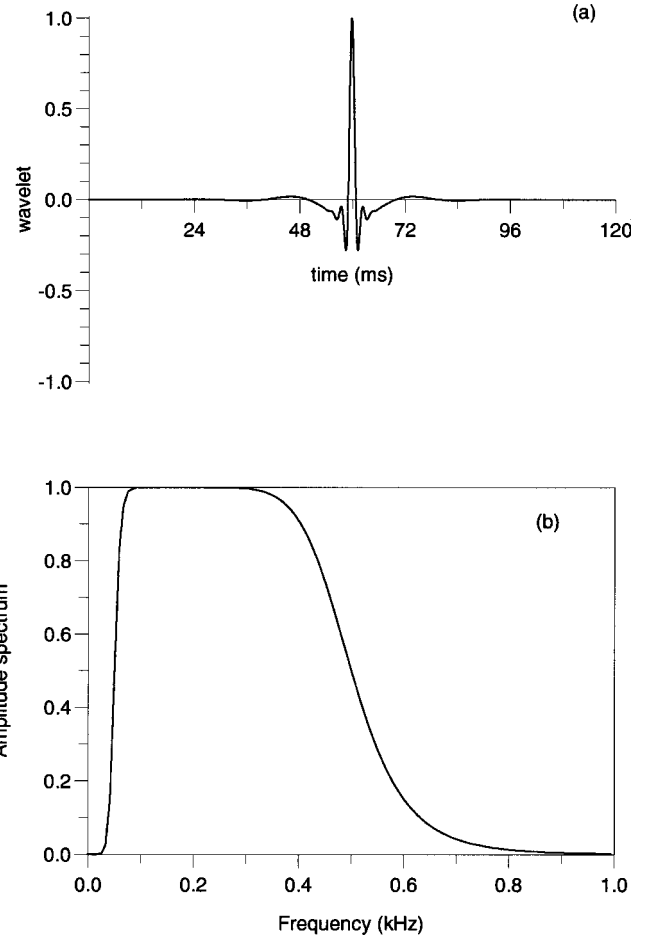


FIG. 9. Time history (a) and Fourier transform (b) of the Butterworth wavelet used to simulate flexural waves.

$$\omega^2 = c_0^2 R_F^2 k^4,$$

has the solutions

$$k = \pm \sqrt{\frac{\omega}{c_0 R_F}}, \quad \text{and} \quad k = \pm i \sqrt{\frac{\omega}{c_0 R_F}}, \quad (70)$$

which correspond to a propagating mode and a static mode, respectively. The phase velocity of the propagating modes is given by

$$V_p = \sqrt{2\pi R_F c_0 f}, \quad \text{and} \quad V_{p \max}/V_{p \min} = \sqrt{f_{\max}/f_{\min}}.$$

In principle, the minimum and maximum velocities propagating in the drill string are 262 and 914 m/s (pipes), and 280 and 978 m/s (joints), respectively. The wavelength is

$$\lambda = \sqrt{2\pi R_F c_0 / f},$$

which yields minimum and maximum wavelengths for the pipe section of 1.5 and 5.24 m, respectively. These values are much larger than the radius of gyration of the pipes (0.043 m), a necessary condition for the validity of the theory.¹⁴ On the other hand, the group velocity is twice the phase velocity.¹⁴

The same mesh and modeling parameters of the first example are used here, and due to less stringent conditions concerning algorithm stability, the wave field is computed with a time step of $10 \mu\text{s}$.

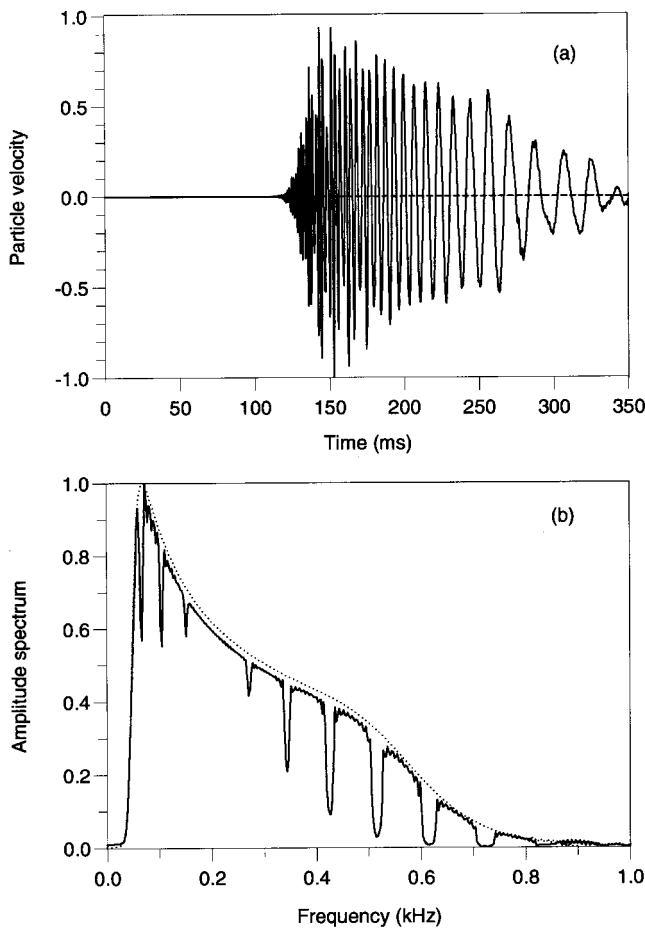


FIG. 10. Time history (a) and Fourier transform (b) of the flexural wave propagated along ten tool joints (see Fig. 1). The dotted line is the amplitude spectrum of the flexural wave in the absence of coupling joints.

Figure 10 shows the particle velocity \dot{w} (a) and its Fourier transform (b). The dotted line is the amplitude spectrum of the flexural wave in the absence of coupling joints. The transform was made using a sampling interval of $400 \mu\text{s}$ and 924 points. Since source and receiver are 126.73 m apart, since the maximum group velocity is approximately 1828 m/s (pipes), and since the source delay is approximately 50 ms, the first break arrives at nearly 120 ms, as can be verified in Fig. 10(a). Moreover, high-frequency energy (short wavelengths) arrives earlier than low-frequency energy, in agreement with the prediction of the dispersion equation. The spectrum indicates that high-frequency energy has been lost. Actually, the energy has been distributed between the propagation and static modes, and the $\sqrt{\omega}$ dependence of the static-mode attenuation factor [see Eq. (70)] explains the dissipation of the high-frequency components. On the other hand, Fig. 10(b) reveals the presence of stopbands. Snapshots of the particle velocity at 120 (a) and 180 ms (b) are shown in Fig. 11, where the arrow and white dot indicate the source and receiver locations, respectively. As can be appreciated, the high-frequency energy precedes the low-frequency energy, and the width of the signal increases with time due to the velocity dispersion effect.

In the last example, we consider coupling between the axial and the flexural motions, corresponding to the drill string of the first example (Fig. 1), where the source is an

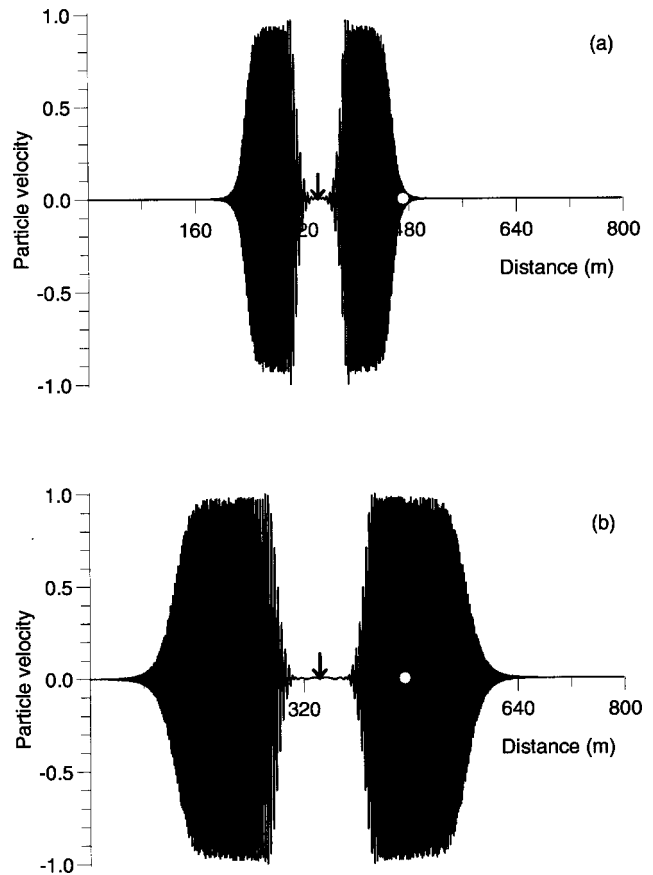


FIG. 11. Snapshots of the flexural wave at 120 (a) and 180 ms (b) in the absence of tool joints. The arrow indicates the source and the white dot the receiver.

axial force. The problem is solved by using the equations obtained by Drumheller⁹ [see Eqs. (48) and (49), respectively]. The radius of curvature of the drill string, r_b , is constant and equal to 120 times the radius of gyration of the pipes. Figure 12 shows the wave field, where the (a) corresponds to the flexural particle velocity \dot{w} and (b) to the extensional particle velocity v . The lateral motion represents a substantial loss of energy from the axial motion. This example is only intended to provide an idea of eventual capabilities of the modeling algorithm. An extensive analysis of coupling and energy exchange will be carried out in a future work.

VI. CONCLUSIONS

We presented the basic theory and algorithm for simulating the different vibrations' modes propagating in drill strings. A set of examples illustrates the versatility of the numerical algorithm: simulation of stopbands in axial and torsional wave propagation, generation of stress waves by piezoelectric transducers, mode attenuation, use of an adaptive mesh for modeling the shape of the coupling joints, flexural mode dispersion and dissipation, and coupling to the axial mode.

The modeling is the basis for further research on acoustic telemetry, such as in the Seisbit[®] method: in particular, simulation of coupled axial, torsional, and lateral vibrations, inclusion of nonlinear back-interaction of lateral bending on

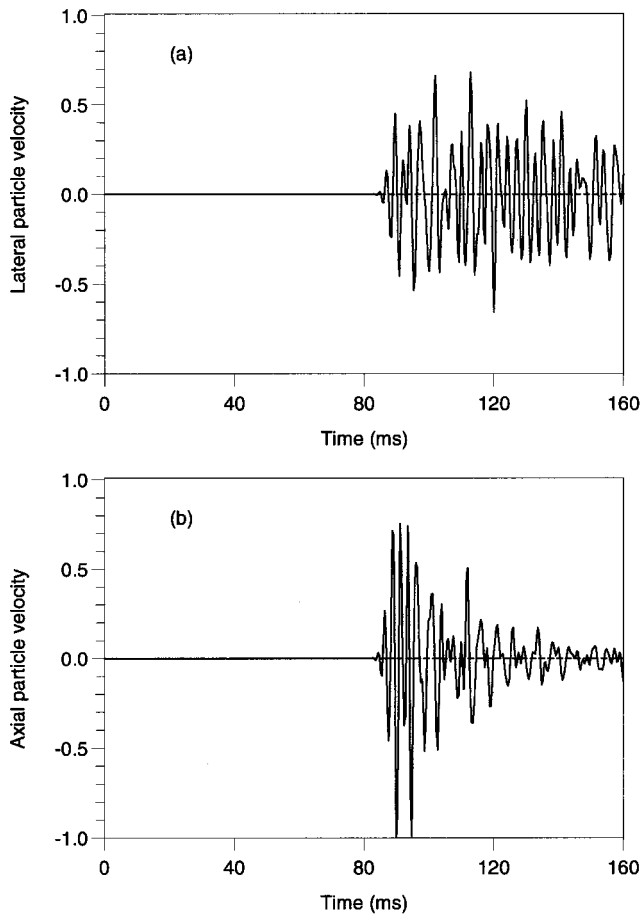


FIG. 12. Flexural (a) and extensional (b) particle velocities \dot{w} and \dot{v} caused by an axial force, corresponding to the model illustrated in Fig. 1.

the axial torsional waves; modeling of boundary conditions, such as rock-bit interaction, allowing the simulation of bit-bounce, rate-of-penetration, stick-slip oscillations, and torque reversals; modeling dual bending modes; focusing of lateral vibrations at the neutral point, etc. Moreover, the algorithm can be implemented in a more complex context, where the whole drill string/drive system is simulated.²²

ACKNOWLEDGMENTS

Thanks to Fabio Cavallini and Géza Seriani for important technical comments.

APPENDIX: WAVE PROPAGATION IN A PIEZOELECTRIC SOLID

Let us assume for simplicity a lossless piezoelectric medium. Such a medium is characterized by the constitutive equations (Ref. 11, p. 274),

$$\mathbf{T} = \mathbf{c}:\mathbf{S} - \mathbf{e} \cdot \mathbf{E}, \quad (\text{A1})$$

$$\mathbf{D} = \mathbf{e}:\mathbf{S} + \boldsymbol{\epsilon} \cdot \mathbf{E}, \quad (\text{A2})$$

where \mathbf{T} is the 6×1 stress vector, \mathbf{S} is the 6×1 strain vector, \mathbf{D} is the 3×1 electric displacement vector, and \mathbf{E} is the 3×1 electric field vector; the dot and the double dot denote the scalar and double scalar products, as defined by Auld.¹¹ Let us assume a medium classified as hexagonal $6mm$, with its symmetry axis coinciding with the z -direction. The stiff-

ness, dielectric, and piezoelectric matrices are given by

$$\mathbf{c} = \begin{pmatrix} c_{11} & c_{12} & c_{13} & 0 & 0 & 0 \\ c_{12} & c_{11} & c_{13} & 0 & 0 & 0 \\ c_{13} & c_{13} & c_{33} & 0 & 0 & 0 \\ 0 & 0 & 0 & c_{44} & 0 & 0 \\ 0 & 0 & 0 & 0 & c_{44} & 0 \\ 0 & 0 & 0 & 0 & 0 & c_{66} \end{pmatrix}, \quad (\text{A3})$$

where $c_{66} = c_{11} - 2c_{12}$,

$$\boldsymbol{\epsilon} = \begin{pmatrix} \epsilon_{xx} & 0 & 0 \\ 0 & \epsilon_{xx} & 0 \\ 0 & 0 & \epsilon_{zz} \end{pmatrix}, \quad (\text{A4})$$

and

$$\mathbf{e} = \begin{pmatrix} 0 & 0 & 0 & 0 & e_{x5} & 0 \\ 0 & 0 & 0 & e_{x5} & 0 & 0 \\ e_{z1} & e_{z1} & e_{z3} & 0 & 0 & 0 \end{pmatrix}, \quad (\text{A5})$$

respectively.

In the absence of sources and conduction currents, Newton's and Maxwell's equations can be written in compact form as

$$\nabla \cdot \mathbf{T} = \rho \partial_{tt} \mathbf{u}, \quad -\nabla \times \mathbf{E} = \mu \partial_t \mathbf{H}, \quad \nabla \times \mathbf{H} = \partial_t \mathbf{D}, \quad (\text{A6})$$

where \mathbf{u} is the elastic displacement vector, \mathbf{H} is the magnetic field vector, ρ is the density, μ is the magnetic permeability, and

$$\nabla \cdot = \begin{pmatrix} \partial_x & 0 & 0 & 0 & \partial_z & \partial_y \\ 0 & \partial_y & 0 & \partial_z & 0 & \partial_x \\ 0 & 0 & \partial_z & \partial_y & \partial_x & 0 \end{pmatrix}, \quad (\text{A7})$$

$$\nabla \times = \begin{pmatrix} 0 & -\partial_z & \partial_y \\ \partial_z & 0 & -\partial_x \\ -\partial_y & \partial_x & 0 \end{pmatrix}.$$

Assume that a uniform z -propagating plane wave exists in the medium. Then, $\partial_x = \partial_y = 0$ and substitution of the constitutive equations (A1) and (A2) into the dynamical equations (A6) yields

$$c_{44} \partial_{zz} u_1 - e_{x5} \partial_z E_1 = \rho \partial_{tt} u_1, \quad (\text{a})$$

$$c_{44} \partial_{zz} u_2 - e_{x5} \partial_z E_2 = \rho \partial_{tt} u_2, \quad (\text{b})$$

$$c_{33} \partial_{zz} u_3 - e_{z3} \partial_z E_3 = \rho \partial_{tt} u_3, \quad (\text{c})$$

$$\partial_z E_2 = \mu \partial_t H_1, \quad (\text{d})$$

$$-\partial_z E_1 = \mu \partial_t H_2, \quad (\text{e}) \quad (\text{A8})$$

$$0 = \mu \partial_t H_3, \quad (\text{f})$$

$$-\partial_z H_2 = e_{x5} \partial_{zt} u_1 + \epsilon_{xx} \partial_t E_1, \quad (\text{g})$$

$$\partial_z H_1 = e_{x5} \partial_{zt} u_2 + \epsilon_{xx} \partial_t E_2, \quad (\text{h})$$

$$0 = e_{z3} \partial_{zt} u_3 + \epsilon_{zz} \partial_t E_3. \quad (\text{i})$$

Assume a phase factor $\exp(i\omega t)$, where ω is the angular frequency, and a spatial phase factor $\exp(-i\omega s z)$, where s is the

slowness in the z -direction. For any field variable, we have

$$\partial_t \rightarrow i\omega \quad \text{and} \quad \partial_z \rightarrow -i\omega s.$$

Using these relations and eliminating the magnetic field components, Eqs. (A8) become

$$\begin{aligned} (c_{44}s^2 - \rho)v_1 + e_{x5}sE_1 &= 0, & \text{(a)} \\ (c_{44}s^2 - \rho)v_2 + e_{x5}sE_2 &= 0, & \text{(b)} \\ (c_{33}s^2 - \rho)v_3 + e_{z3}sE_3 &= 0, & \text{(c)} \\ \mu e_{x5}sv_1 + E_1(s^2 - \mu\epsilon_{xx}) &= 0, & \text{(g)} \\ \mu e_{x5}sv_2 + E_2(s^2 - \mu\epsilon_{xx}) &= 0, & \text{(h)} \\ -se_{z3}v_3 + \epsilon_{zz}E_3 &= 0, & \text{(i)} \end{aligned} \tag{A9}$$

where $\mathbf{v} = \partial_t \mathbf{u}$ is the particle velocity vector. Equations (A9a)(b) and (A9f)(h) give the dispersion equation for the *quasiacoustic* and *quasi-electromagnetic* waves,

$$(s^2 - \mu\epsilon_{x5})(s^2 c_{44} - \rho) - \mu e_{x5}^2 s^2 = 0, \tag{A10}$$

with \mathbf{v} and \mathbf{E} polarized in the plane perpendicular to the symmetry (poling) axis. On the other hand, Eqs. (A9c) and (A9i) yield the dispersion relation of the *piezoelectrically stiffened acoustic wave*,

$$s^2 \left(c_{33} + \frac{e_{z3}^2}{\epsilon_{zz}} \right) = \rho, \tag{A11}$$

with \mathbf{v} and \mathbf{E} polarized along the symmetry (poling) axis. From Eqs. (A8f) and (A8i), this wave mode satisfies $\partial_t H_3 = 0$ and $\partial_t D_3 = 0$, and H_3 and D_3 are both zero, except for time-independent fields that are not of interest. That the electric field has zero curl implies that it can be represented as the gradient of a scalar potential even though it is time-varying, not static. This is called a *quasistatic field*.¹¹

¹D. S. Drumheller, "Attenuation of sound waves in drill strings," J. Acoust. Soc. Am. **94**(4), 2387–2396 (1993).

²D. S. Drumheller and S. D. Knudsen, "The propagation of sound waves in

drill strings," J. Acoust. Soc. Am. **97**(4), 2116–2125 (1995).

³E. L. Hixon, US Patent 3,252,225 (1966).

⁴W. H. Cox and P. E. Chaney, "Telemetry system," US Patent No. 4,293,936 (1981).

⁵H. E. Sharp and M. A. Smither, "Borehole acoustic telemetry system with phase shifted signals," US Patent 4,562,559 (1985).

⁶F. Miranda, L. Aleotti, F. Abramo, F. Poletto, A. Craglietto, S. Persoglia, and F. Rocca, "Impact of seismic while drilling technique on exploration wells," First Break **14**, 55–68 (1996).

⁷L. Aleotti, F. Poletto, F. Miranda, P. Corubolo, F. Abramo, and A. Craglietto, "Seismic while-drilling technology: Use and analysis of the drill-bit seismic source in a cross-hole survey," Geophys. Prospect. **47**, 25–39 (1999).

⁸T. G. Barnes and B. R. Kirkwood, "Passbands for acoustic transmission in an idealized drill string," J. Acoust. Soc. Am. **51**, 1606–1608 (1972).

⁹D. S. Drumheller, "Extensional stress waves in one-dimensional elastic waveguides," J. Acoust. Soc. Am. **92**(6), 3389–3402 (1992).

¹⁰J. M. Carcione, D. Kosloff, and R. Kosloff, "Wave propagation simulation in a linear viscoelastic medium," Geophys. J. R. Astron. Soc. **95**, 597–611 (1988).

¹¹B. A. Auld, *Acoustic Fields and Waves in Solids* (Krieger, Malabar, Florida, 1990).

¹²J. M. Carcione, "Ground penetrating radar: Wave theory and numerical simulation in lossy anisotropic media," Geophysics **61**, 1664–1677 (1996).

¹³A. E. H. Love, *A Treatise on the Mathematical Theory of Elasticity* (Cambridge University Press, Cambridge, 1952).

¹⁴H. Kolsky, *Stress Waves in Solids* (Clarendon, Oxford, 1953).

¹⁵P. M. Morse and K. U. Ingard, *Theoretical Acoustics* (Princeton University Press, Princeton, NJ, 1986).

¹⁶W. C. Chin, *Wave Propagation in Petroleum Engineering* (Gulf, □□, 1994).

¹⁷D. S. Drumheller, "Coupled extensional and bending motion in elastic waveguides," Wave Motion **17**, 319–327 (1993).

¹⁸D. S. Drumheller, "Acoustic properties of drill strings," J. Acoust. Soc. Am. **85**(3), 1048–1064 (1989).

¹⁹N. J. C. Lous, S. W. Rienstra, and I. J. B. F. Adan, "Sound transmission through a periodic cascade with application to drill pipes," J. Acoust. Soc. Am. **103**(5), 2302–2311 (1998).

²⁰D. Kosloff, M. Reshef, and D. Loewenthal, "Elastic wave calculations by the Fourier method," Bull. Seismol. Soc. Am. **74**, 875–891 (1984).

²¹J. M. Carcione, "A 2D Chebyshev differential operator for the elastic wave equation," Comput. Methods Appl. Mech. Eng. **130**, 33–45 (1996).

²²J. D. Jansen and L. van den Steen, "Active damping of self-excited torsional vibrations in oil well drill strings," J. Sound Vib. **179**(4), 647–668 (1995).